

10

Pas de H3

64

Equatorially trapped Rossby-gravity wave propagation in the Gulf of Guinea

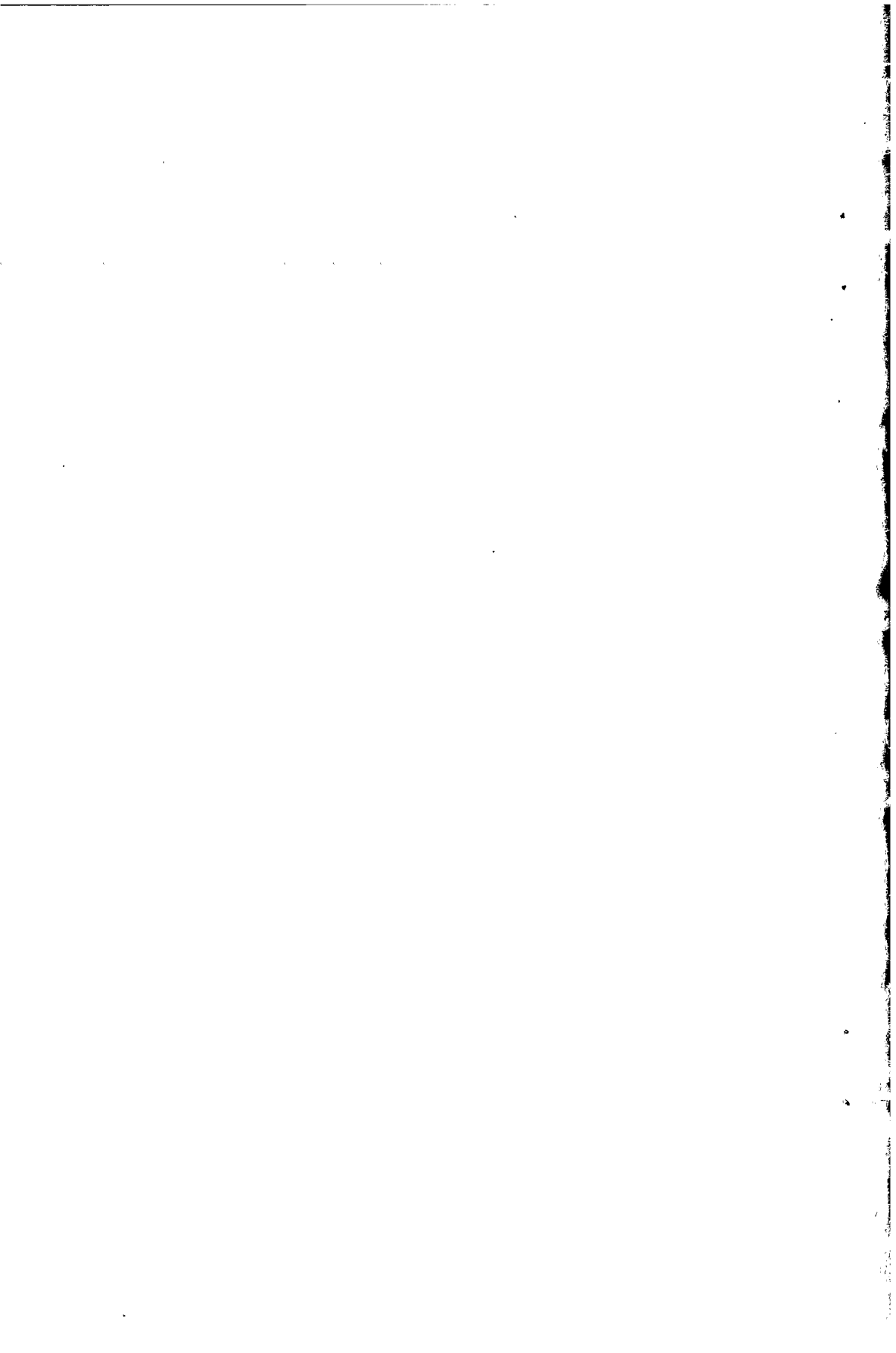
R. H. WEISBERG, A. HORIGAN, AND C. COLIN ^{mistiau}

Antenne O. R. S. T. O. M.
CENTRE OCÉANOLOGIQUE DE BRETAGNE
BUREAU CALCUL

Fonds documentaire IRD
Cot : B * 26640 Ex : unique

REPRINT FROM
SEARS FOUNDATION: JOURNAL OF MARINE RESEARCH
Volume 37, Number 1, February, 1979. Pp. 67-86





Equatorially trapped Rossby-gravity wave propagation in the Gulf of Guinea

by R. H. Weisberg,¹ A. Horigan,² and C. Colin³

ABSTRACT

Equatorially trapped vertically propagating Rossby-gravity waves have been observed in the Gulf of Guinea. Analyses of their kinematics, dynamics, and energetics are presented. The particular packet considered had band central values for period, zonal wavelength, and vertical wavelength of 31 days, 1220 km, and 990 m respectively. The phase propagation was westward and upward while the energy flux was eastward and downward. The calculated trapping (*e*-folding) scale was 210 km. Therefore, the waves were unaffected by the zonal African coast situated some 500 km to the north. The waves were linear, energetic, and persistent showing that the equator is a waveguide for planetary scale oscillations.

1. Introduction

Theory suggests that the equator may serve as a waveguide for planetary scale oscillations. This paper presents observations of equatorially trapped waves in the Gulf of Guinea (the eastern equatorial Atlantic). It is based upon a collaborative U.S.–French field experiment consisting of moored current meter and hydrographic measurements which began in June, 1976. Eighteen months of continuous velocity data have revealed fairly regular (though frequency and amplitude modulated) oscillations with an approximate time scale of one month. The six month subsample spanning July 1977–January 1978 provided sufficient three dimensional coverage to ascertain the structure and properties of these dominant oscillations accounting for some 2/3 of the meridional component variance. We conclude that they are packets of vertically propagating equatorially trapped Rossby-gravity waves.

The paper is developed in 9 sections. Section 2 reviews the relevant theory. Section 3 presents the data. Section 4 discusses the kinematics of the observed flow field. A wavenumber vector is estimated in Section 5. Section 6 then compares the dynamics of the Rossby-gravity wave model with the observations. Since the observations agree very well with the wave model, the dispersion relation is employed in

1. Department of Marine Science and Engineering, North Carolina State University, Raleigh, North Carolina, 27650, U.S.A.

2. Graduate School of Oceanography, University of Rhode Island, Kingston, Rhode Island, 02882, U.S.A.

3. Centre de Recherches Oceanographiques, B.V.P. 18 Abidjan, Ivory Coast.

Section 7 to expand upon the energetics of the oscillations. The results are discussed and summarized respectively in Sections 8 and 9.

2. Background

Equatorial trapping, or waveguiding, is related to the vanishing of the Coriolis parameter at the equator and the attendant symmetric planetary vorticity gradient. The vanishing Coriolis parameter also decreases the time scale and increases the length scale for baroclinic motions. These ideas were embodied in Lighthill's (1969) attempt to account for the seasonal development of the Somali current by the zonal energy flux of equatorially trapped waves. Moore and Philander (1977) and Holton (1975) review equatorial wave theory for the ocean and atmosphere respectively.

Matsuno (1966) described equatorial waves on an unbounded β -plane in terms of zonally propagating meridional and vertical modes. For a given baroclinic (vertical) mode, four classes of waves exist: 1) inertia-gravity, 2) Rossby, 3) Rossby-gravity, and 4) Kelvin waves. Associated with each of these classes are discrete meridional mode numbers n . The Kelvin wave is a special case formally associated with $n = -1$. It has no meridional velocity component (v) and its zonal velocity component (u) and pressure perturbation (p) fields decay away from the equator as $\exp(-\beta y^2/2(gh)^{\frac{1}{2}})$ where h is the equivalent depth for the baroclinic mode. The e -folding distance is $y = (2/\beta)^{\frac{1}{2}}(gh)^{\frac{1}{4}}$; therefore, the equivalent depth (decreasing with increasing baroclinic mode) controls the trapping scale. The Rossby-gravity wave ($n = 0$) is the gravest meridional mode and both inertia-gravity and Rossby waves exist for $n \geq 1$. The eigenfunctions for the meridional modes consist of Hermite functions (i.e. Hermite polynomials multiplied by the exponential decay term for the Kelvin wave above). Each meridional mode has distinct symmetry properties about the equator. Even modes ($n = 0, 2, \dots$) are symmetric in v and anti-symmetric in u and p . Opposite symmetry properties apply for odd modes ($n = 1, 3, \dots$). Therefore, the eigenfunctions for an unbounded ocean either have nodes or relative extrema (maxima or minima) on the equator, and the equator is the line of symmetry.

The geometric dispersion relation of the Matsuno (1966) solution does not conveniently represent vertically propagating waves. Hence, Lindzen and Matsuno (1968) considered waves forced at a specific zonal wavenumber component k and frequency σ in order to account for the vertical wavenumber component m observed by Yanai and Maruyama (1966) in the lower stratosphere. Philander (1978a) adopted a similar approach for studying the behavior of oceanic equatorial waves. The linear equations for momentum and mass conservation on a β -plane without dissipation are separable into vertical and horizontal parts. Using Philander's (1978a) notation, the dimensional equations for the separated vertical and meridional velocity components are:

$$W_{zz} + (N^2/gh) W = 0 \quad 2.1$$

and

$$V_{yy} + (\sigma^2/gh - k^2 - \beta k/\sigma - \beta^2 y^2/gh) V = 0 \quad 2.2$$

where $(gh)^{\frac{1}{2}}$ is the separation constant, and all dependent variables are proportional to $\exp\{i(kx - \sigma t)\}$. Equation 2.2 has solutions bounded at $y = \pm \infty$ provided that:

$$\sigma^2/gh - k^2 - \beta k/\sigma = (2n + 1) \beta/(gh)^{\frac{1}{2}} \quad 2.3$$

n being the integer meridional mode number. If equation 2.1 is solved in accordance with an observed buoyancy frequency profile then vertical modes result and h is the equivalent depth for a given mode. Alternatively, an effective equivalent depth follows from the intrinsic dispersion relation (equation 2.3) for a specified σ , k , and n :

$$(gh)^{\frac{1}{2}} = \frac{-\beta(2n + 1) \pm \{\beta^2(2n + 1)^2 + 4(k^2 + \beta k/\sigma)\sigma^2\}^{\frac{1}{2}}}{2(k^2 + \beta k/\sigma)}, \quad 2.4$$

and a local intrinsic vertical wavenumber component m then follows from equation 2.1:

$$m = \pm N/(gh)^{\frac{1}{2}}. \quad 2.5$$

Philander (1977) also treated equatorial waves in the presence of a zonal boundary north of the equator. Specific application was made to the Gulf of Guinea where the horizontally unbounded wave results of Lindzen and Matsuno (1968) may be significantly modified if the zonal coast lies equatorward of the turning latitude. Since the boundary conditions are no longer symmetric in this occurrence (i.e., $v = 0$ at $y = +y_0$ and $y = -\infty$ as opposed to $v = 0$ at $y = \pm \infty$) the solutions lose their symmetry about the equator. Furthermore, two additional meridional wave modes are possible due to the overlapping radii of deformation for the equatorial and coastal regions: 1) a mixed Rossby-Kelvin and 2) a mixed Kelvin-gravity wave. Therefore, the tropical Atlantic (at least the Gulf of Guinea which occupies half of it) may respond differently to forcing than the Pacific or Indian Oceans. Whether or not this occurs depends upon the trapping scale which is controlled by the equivalent depth. If the geometric baroclinic mode equivalent depth is small (vertical modes higher than the second), or if the intrinsic effective equivalent depth for vertically propagating waves is small, then the zonal coast is effectively at infinity and the solutions simplify to the unbounded case. Equations 2.4 and 2.5 will be used in section 6 with this problem in mind.

3. The data

The positions of the subsurface equatorial and coastal moorings are shown in Figure 1. Data from the four locations on the triangular equatorial array listed in Table 1 will be presented. These data were recorded on A.M.F. Vector Averaging

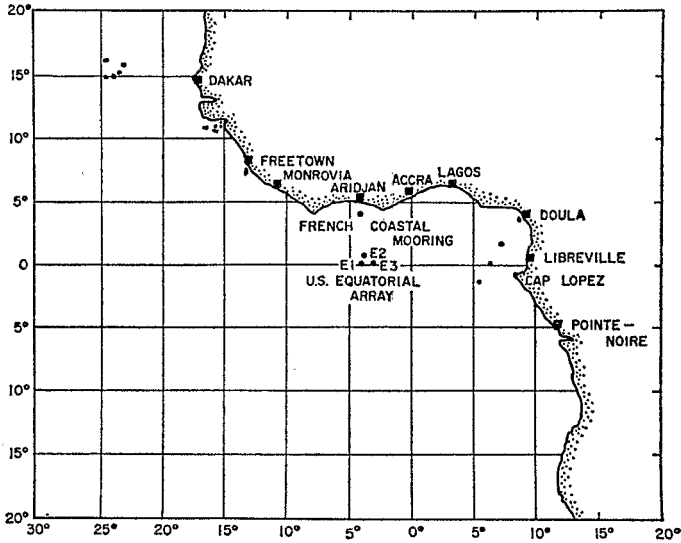


Figure 1. Subsurface mooring positions.

Table 1. The locations of records used in this study.

Position	Latitude, Longitude	Depth, m
E11	00° 01.1' N, 04° 16.0' W	579
E22	00° 32.0' N, 03° 56.4' W	610
E31	00° 02.7' S, 03° 08.6' W	568
E33	00° 02.7' S, 03° 08.6' W	868

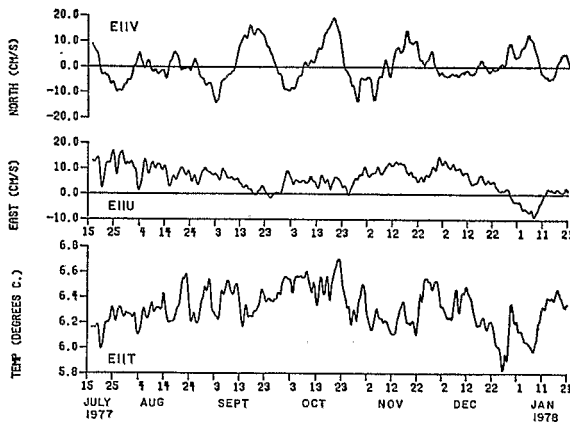


Figure 2. Low pass filtered velocity component and temperature for E11.

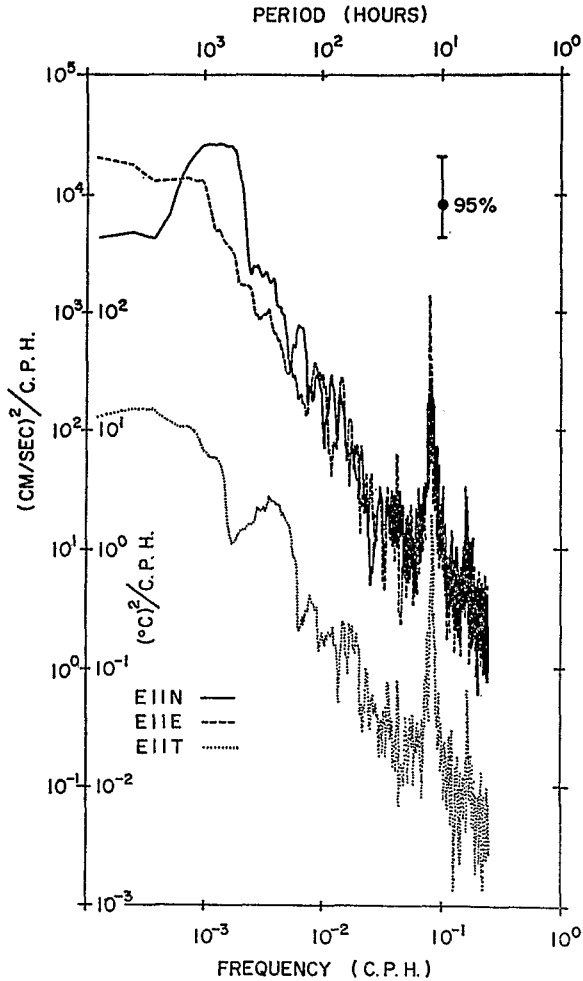


Figure 3. Velocity component and temperature variance spectra for E11. The 95% confidence interval for random errors with 12 degrees of freedom is given in the upper right.

Current Meters with a sampling interval of 15 min. and a sampling duration of 15 July, 1977 to 22 January, 1978.

Figure 2 shows the low pass filtered u and v velocity components and temperature (T) from record E11. The v component fluctuates in a sinusoidal fashion about a zero mean and is uncorrelated with either u or T . The spectra for these time series are shown in Figure 3. Note the pronounced peak in v centered upon an approximate one month periodicity followed by a cut-off at longer time scales. This behavior is atypical of deep ocean spectra and except for the whitening due to topographic Rossby waves shown by Thompson (1977), we are unaware of similar observations at extra-equatorial latitudes. In contrast, both the u and T spectra exhibit the typical

Table 2. Velocity component means and total variances along with the percentage of v component variance between 1024-546 hours and the corresponding r.m.s. amplitudes.

Position	\bar{u} cm/sec	\bar{v} cm/sec	$(u-\bar{u})^2$ cm ² /sec ²	$(v-\bar{v})^2$ cm ² /sec ²	% (1024-546 hr)	$v_{r.m.s.}$ (1024-546 hr)
E11	5.9	0.9	30.1	49.8	66	5.7
E22	2.5	0.4	35.4	56.2	64	6.0
E31	6.3	0.7	49.4	40.5	67	5.2
E33	-1.2	-0.3	63.1	48.0	67	5.6

“red” behavior at low frequency. The velocity component variances for the records E11, E22, E31, and E33 are listed in Table 2. Roughly 2/3 of the v component variance is contained within the band centered upon the time scale of 745 hrs. (31 days) and spanning 1024-546 hrs. The qualitative nature of this dominant process may be visualized with the aid of the velocity vector time series shown in Figure 4. The motions resemble a wavy packet undergoing about three sinusoidal oscillations which are highly coherent over the entire array (126 km zonally, 57 km meridionally, and 300 m vertically).

4. Kinematics of the flow field

The time dependent motions directly on the equator tend to be rectilinear. This is evident by the lack of polarization preference in the anticlockwise (+) and clock-

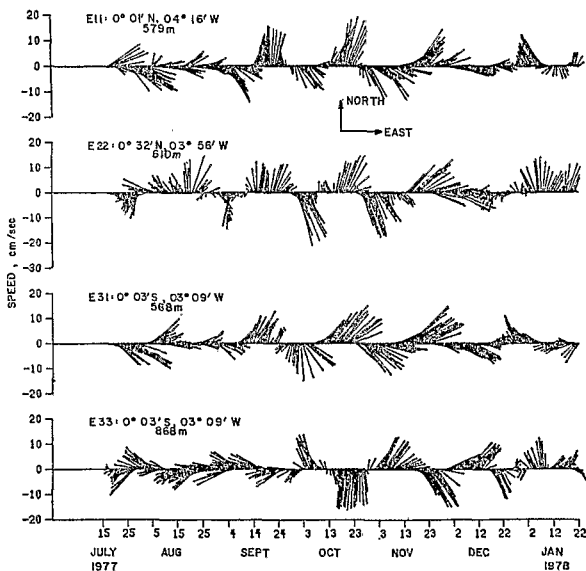


Figure 4. Low pass filtered velocity vector time series for E11, E22, E31, and E33. Vectors are plotted every 8 hours.

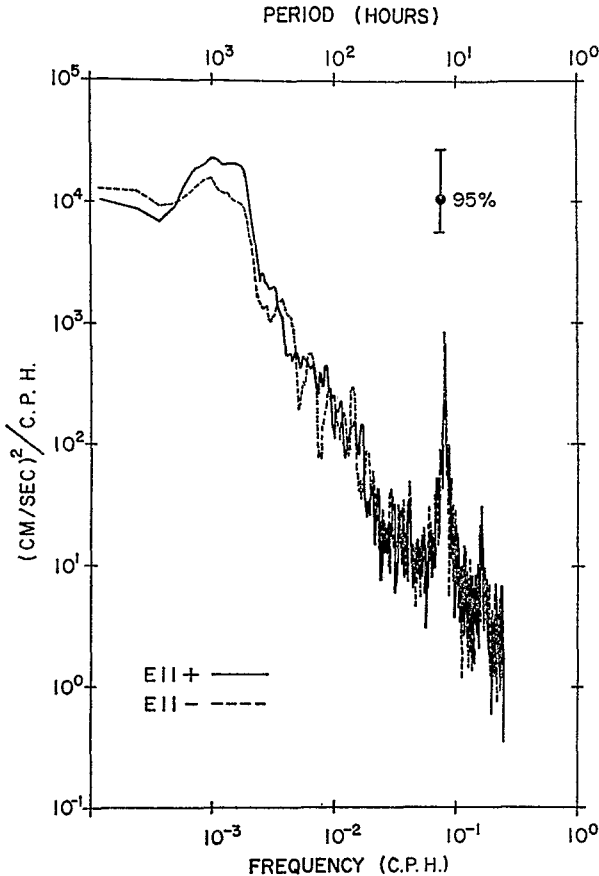


Figure 5. Anticlockwise (+) and clockwise (−) velocity variance spectra for E11. The 95% confidence interval for random errors with 12 degrees of freedom is given in the upper right.

wise (−) rotary spectra shown in Figure 5. Focusing now on the dominant low frequency process, Figure 6 gives eight descriptors of the flow field for an equatorial and an off-equatorial record: E33 and E22 respectively. From top to bottom they are: a) $\log v$ component energy density, b) maximum and minimum coherence squared between orthogonal velocity components, c) hodograph ellipse stability, d) principal axis orientation, e) semi-minor to semi-major axis ratio, f) meridional velocity component and temperature coherence squared, and g) zonal velocity component and temperature coherence squared. The solid lines are for the equatorial record E33 and the dashed lines are for the off-equatorial (57 km north of the equator) record E22. The energy density peak delineates the frequency band of interest. Inspection of the unaveraged periodograms from all of the records (not shown) clearly showed the band center to be at 2.34×10^{-6} rad/sec which corresponds to

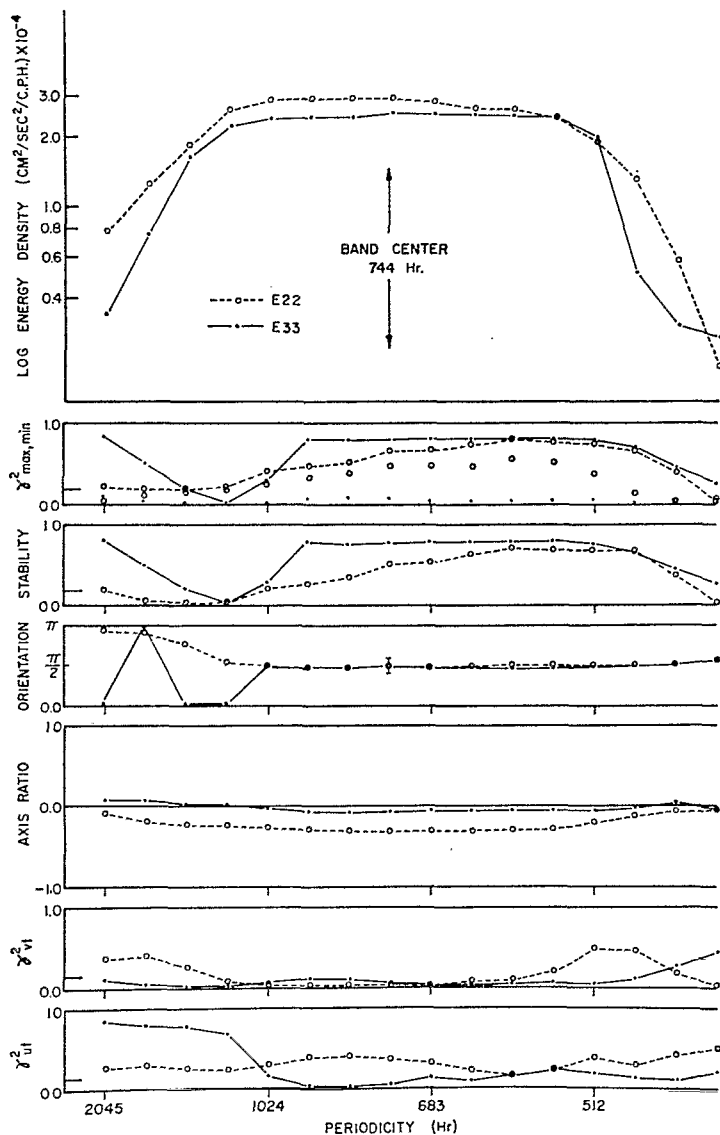


Figure 6. Kinematical descriptors of the dominant water particle motions at the "off-equator" location E22 and at the "on-equator" location E33. Corresponding to 12 degrees of freedom the 90% significance level for coherence squared and stability are given by horizontal ticks on the ordinates, and the 90% confidence interval for orientation is indicated at the band central frequency.

a periodicity of 31 days. All of the v component spectra: E11, E22, E31, and E33 were nearly identical over this frequency band.

The minimum and maximum coherencies are measures of the orderliness or wavi-

ness of the motions. They are coherencies between orthogonal velocity components relative to the principal axis of the velocity hodograph ellipse and relative to axes rotated 45 degrees from the principal axes respectively. Detailed discussions of the velocity hodograph model for vector time series are given by Fofonoff (1969), Gonella (1972), and Mooers (1973). High maximum and minimum coherencies signify a coherent elliptical oscillation. High maximum and low minimum coherencies signify a coherent rectilinear oscillation. The maximum coherency for the equatorial record E33 increases sharply upon entering the band from the low frequency end to a value of about 0.8 and then decreases sharply upon leaving the band at the high frequency end. The minimum coherency on the other hand is nearly zero across the entire band. The maximum coherency for the off equator record E22 behaves very similarly to E33; however, unlike the on-equator record, the minimum coherency also increases to a maximum value within the band. Coherency analysis therefore suggests that the motions within this band are rectilinearly coherent on the equator and elliptically coherent 57 km north of the equator.

The next two descriptors, the stability and orientation, may be viewed together. The stability is the coherence squared between the anticlockwise and clockwise circular motions which sum together to give the resultant elliptical motions and the orientation is the directionality of the ellipse semimajor axis. Again, upon entering the band from the low frequency side and leaving at the high frequency side stability increases sharply and then decreases sharply for both the on-equator and off-equator records. When the stability is high, the orientation of the semi-major axis is clearly $\pi/2$ or north.

The axis ratio is a measure of the eccentricity of the ellipse. It is nearly zero across the band for the on-equator record and -0.30 at the band center for the off-equator record. The sign indicates clockwise polarization. Both the sign and magnitude will serve as an important dynamical check later.

The velocity component/temperature coherence shows that both u and v are uncorrelated to T on the equator while off the equator u and T are correlated.

Putting these pieces of information together, we can summarize the kinematics of the flow field associated with the dominant low frequency process in the following manner.

a. It is centered upon a time scale of 31 days (745 hours) roughly spanning the time scales of 1024-546 hours.

b. The motions within this band are highly coherent and rectilinear on the equator while being highly coherent and elliptical (clockwise polarized) with a well defined axis ratio off the equator.

c. The water particle paths have their semi-major axis oriented north-south both on and off the equator.

d. The equator is a node for u and T .

Combining b, c, and d suggests that the water particle motions are symmetric in

Table 3. The directional cosine matrix and the phase difference/displacement magnitude column vector used in the three dimensional wavenumber vector (k, l, m) analysis. The rows from top to bottom correspond to the instrument pairs E11-E22, E22-E31, E11-E31 respectively.

$$\begin{pmatrix} 0.534 & 0.845 & -0.519 \times 10^{-3} \\ 0.828 & -0.561 & 0.414 \times 10^{-3} \\ 0.999 & -0.032 & 0.793 \times 10^{-4} \end{pmatrix} \begin{pmatrix} k \\ l \\ m \end{pmatrix} = \begin{pmatrix} -0.628 \times 10^{-2} \\ -0.225 \times 10^{-2} \\ -0.530 \times 10^{-2} \end{pmatrix}$$

ν and anti-symmetric in u with the equator serving as the line of symmetry for the time scales defined by a .

5. Wavenumber analysis

Given the kinematical description in view of the theoretical background it is hypothesized that the observed oscillations are due to symmetric equatorially trapped waves. The associated wavenumber vector may be estimated by equating its projections onto the instrument pair displacement vectors with the phase differences between paired instruments. In matrix form this is:

$$C K = P, \quad 5.1$$

where C is the 3×3 directional cosine matrix for the angles made between the instrument pair displacement vectors and the coordinate axes, the column vector K is the unknown wavenumber, and the column vector P consists of phase differences divided by displacement magnitudes. Equation 5.1 was applied to the three dimensional circuit connecting records E11, E22, and E31. Table 3 outlines the calculation at the band central frequency. The phase differences were determined from the ν component Fourier coefficients and the resulting zonal, meridional, and vertical wavenumber components are respectively: $k = -5.98 \times 10^{-3} \text{ km}^{-1}$, $l = 0$, and $m = 6.15 \text{ km}^{-1}$.

The fact that $l = 0$ supports the equatorial wave hypothesis. This enables us to recompute k and m directly from zonally and vertically separated instruments without additional extraneous noise introduced by meridional separation. Figure 7 shows the coherency between ν components separated zonally by 126 km (E1131N) and vertically by 300 m (E3133N). The coherence squared is very high across the band of interest in both cases (it was similarly high for the on-off equator pairs). The negative values for phase show that oscillations at E31 lead those at E11 and that oscillations at E33 lead those at E31 i.e., the sense of phase propagation is westward and upward as calculated above. The vertical wavenumber component at the band center was computed directly from records E31 and E33 on the same mooring. The zonal wavenumber component was then estimated from record pairs E11-E31 and E11-E33; each being corrected for vertical propagation via a two dimensional application of equation 5.1. The two zonal component estimates (differing by 17%)

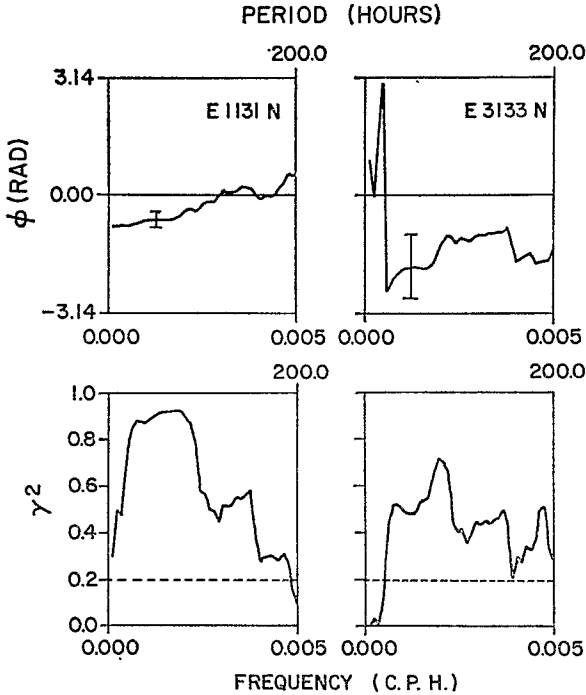


Figure 7. Coherency between v components separated zonally by 126 km (E11 and E31) and separated vertically by 300m (E31 and E33). Corresponding to 12 degrees of freedom, the 90% significance level for coherence squared is given by the dashed lines and the 90% confidence interval for the phase differences are indicated at the band central frequency.

were then averaged. Table 4 gives the final estimates for the wavenumber vector, phase speeds, and wavelengths along with their 90% confidence limits. Note that the wavenumber vector is nearly vertical.

As a kinematical consistency test of the wave hypothesis, we've computed the line integral of $K \cdot \delta r$ around each of the four circuits encompassing the instruments. This quantity should be zero since wavenumber vectors are irrotational. The tests are shown in Figure 8. They all pass the null hypothesis within the band of interest while they diverge abruptly upon leaving the band at the high and low frequency

Table 4. Estimated band central ($\sigma = 2.34 \times 10^{-6}$ radians/sec) wavenumber, phase speed, and wavelengths; and their approximate 90% confidence intervals for random errors (in parentheses).

	zonal component	vertical component
Wavenumber	$-5.16 (\pm 1.95) \times 10^{-8} \text{ km}^{-1}$	$6.34 (\pm 2.91) \text{ km}^{-1}$
Phase speed	$-45 (33 \text{ to } 73) \text{ cm/sec}$	$0.037 (0.025 \text{ to } 0.068) \text{ cm/sec}$
Wavelength	$1220 (880 \text{ to } 1960) \text{ km}$	$990 (680 \text{ to } 1830) \text{ m}$

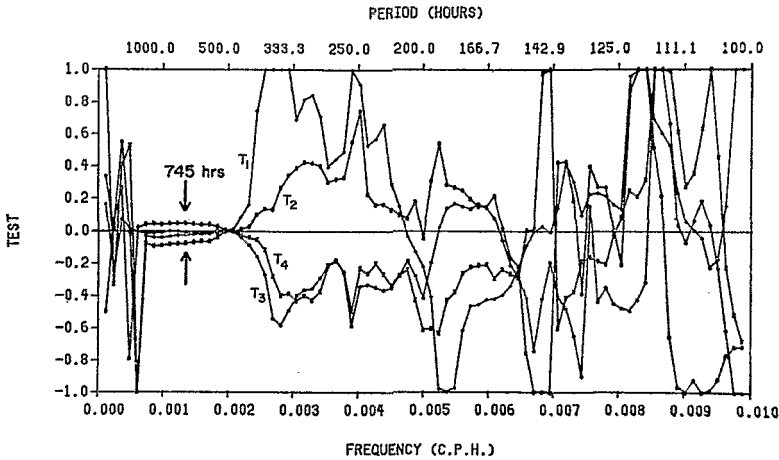


Figure 8. Normalized wavenumber irrotationality tests as a function of frequency. Tests T_1 , T_2 , T_3 , and T_4 correspond to the closed circuits connecting E11, E22, E31; E11, E31, E33; E11, E22, E33; and E22, E31, E33 respectively where:

$$T_i = \sum_j K \cdot \delta r / \sum_i |K \cdot \delta r|.$$

ends. The band of interest is the only portion of the low frequency spectrum where the test shows validity.

6. Dynamics

a. Wavenumber components. Equations 2.4 and 2.5 are related by the separation constant $c = (gh)^{\frac{1}{2}}$. Therefore, a theoretical determination of m follows from an observation of k and vice versa. The observations are consistent with the theory to the extent that the independently observed k and m agree with their theoretical counterparts.

The gravest mode applicable to the observations is the Rossby-gravity wave ($n=0$) for which the dispersion relation reduces to:

$$(gh)^{\frac{1}{2}} = \sigma^2 / (\beta + \sigma k) \quad 6.1$$

At the band central frequency, Table 5 lists the quantities used to determine c from

Table 5. Numerical values used for the band central dynamical calculations.

σ	:	$2.34 \times 10^{-6} \text{ sec}^{-1}$
k	:	$-5.16 \times 10^{-8} \text{ cm}^{-1}$
m	:	$6.34 \times 10^{-6} \text{ cm}^{-1}$
β	:	$2.29 \times 10^{-13} \text{ cm}^{-1} \text{ sec}^{-1}$
g	:	978 cm/sec^2
N_{550m}	:	$0.28 \times 10^{-2} \text{ sec}^{-1}$

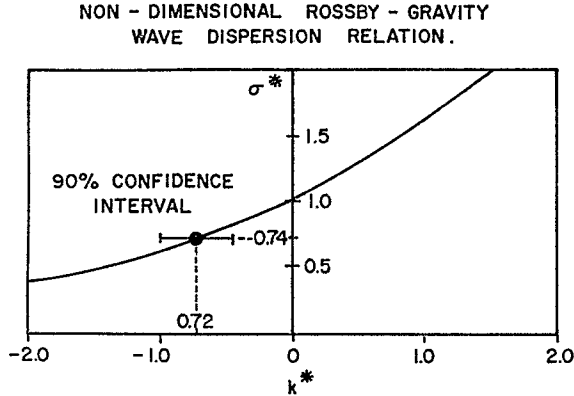


Figure 9. nondimensional Rossby-gravity wave dispersion relation showing the observed σ , k pair (and 90% confidence interval for k) nondimensionalized using the value of c independently determined from the observed m . The observational/theoretical agreement is excellent.

equation 6.1 and m from equation 2.5. The buoyancy frequency was obtained using contemporary data at 4W from the N.O. *Capricorne* and from historical data at 10W during GATE. The resulting values for c and h are 50.6 cm/sec and 2.6 cm respectively which transform into a vertical wavenumber component of 5.53 km^{-1} . This only differs by 13% from the observed vertical wavenumber component (6.34 km^{-1}) and the difference is smaller than the 90% confidence interval for random errors. A second independent determination of the separation constant using equation 2.5 and the observed m results in $c = 44.2 \text{ cm/sec}$. The corresponding theoretical zonal wavenumber component determined via equation 6.1 is $k = -4.50 \times 10^{-3} \text{ km}^{-1}$ which only differs by 12% from the observed value ($-5.12 \times 10^{-3} \text{ km}^{-1}$). To summarize the observational/theoretical wavenumber comparisons the observed σ and k have been nondimensionalized by the time scale $(c\beta)^{-\frac{1}{2}}$ and the length scale $(c/\beta)^{\frac{1}{2}}$ using the independent estimate of c associated with the observed m . The result is plotted on a nondimensional dispersion curve for the Rossby-gravity wave in Figure 9 and the agreement is excellent.

In repeating the above analysis for the next possible choice of meridional mode number ($n=2$) the separation constants were found to be either much too small (inertia-gravity waves) or much too large (Rossby waves) for observational consistency. For this reason and others to follow only the Rossby-gravity wave is relevant to the observations.

b. Meridional structure. The semi-minor to semi-major axis ratio for the Rossby-gravity wave water particle paths is:

$$u_0/v_0 = -\beta y / \{\sigma - (gh)^{\frac{1}{2}}k\} = -\sigma y / (gh)^{\frac{1}{2}} \quad 6.2$$

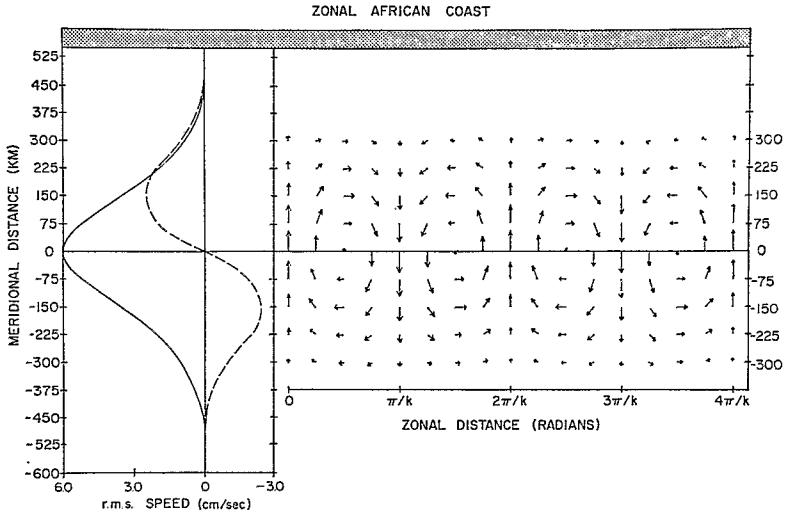


Figure 10. The dimensional Rossby-gravity wave eigenfunctions and a snapshot (at $t=0$) of the associated water particle trajectories relative to the zonal African coast. The equatorial radius of deformation and the e -folding scale for this case are 148 km and 210 km respectively and the observed r.m.s. speed is approximately 6 cm/sec.

The theoretical axis ratios at $y = 57$ km (mooring E2) are -0.27 using $c = 50.6$ cm/sec and -0.30 using $c = 44.2$ cm/sec. These compare remarkably well with the observed axis ratio of -0.30 shown in Figure 6.

The theoretical trapping or e -folding scale of the eigenfunctions is also determined by the separation parameter. It is either 197 km or 210 km depending upon the value of c used. Thus, the observed equatorial oscillations are unaffected by the zonal African coast situated some 500 km away. Observational verification of this is obtained in two ways. First, the kinematics described in section 3 suggest a mode of oscillation centered about the equator, whereas Philander (1977) showed that the coast causes the kinematics to be skewed relative to the equator. Second, we did not observe similar oscillations in the simultaneous coastal mooring records at the same longitude near Abidjan, Ivory Coast.

The meridional structure envisaged by these dynamically consistent results are shown in Figure 10. The relative magnitudes of u and v are shown on the left as a function of y , and a snapshot of the water particle trajectories at the arbitrary time ($t=0$) is shown on the right as a function of x and y .

c. Vertical scaling. The WKB approximation may be used for vertical propagation through a slowly varying medium. This procedure is outlined in Phillips (1977) and the relatively small effective equivalent depth observed suggests that it should apply to the present case as a further consistency check. The pertinent comparison is the

manner in which the horizontal velocity component varies with depth since in a WKB solution v is proportional to $N^{\frac{1}{2}}$, where N is the buoyancy frequency.

The transfer function between two time series gives the amplitude ratio for the coherent portion of the spectrum. This linear least squares error estimate of the amplitude ratio between the meridional velocity components from E31 and E33 at the band central frequency is 0.78. In comparison the square root of the buoyancy frequency ratio at 550 m and 850 m at mooring E3 is 0.89. As a dynamical consistency check in the vertical the observed amplitude ratio is smaller than the WKB amplitude ratio by 12%. The fact that the observed ratio is smaller than the buoyancy frequency ratio may be the result of dissipation, however, the difference is not statistically different from zero at the 90% level using a Fisher F-test.

7. Energetics

a. Group velocity and energy flux. In view of the kinematical and dynamical consistencies shown, we will now utilize the dispersion relation to expand upon the energetics of the wave packet. The group velocity vector follows from equation 6.1:

$$\begin{aligned} \mathbf{C}_g &= \frac{\partial \sigma}{\partial k} \mathbf{i} + \frac{\partial \sigma}{\partial m} \mathbf{k} \\ &= (2\sigma/(gh)^{\frac{1}{2}} - k)^{-1} \{ \sigma \mathbf{i} - (gh)^{\frac{1}{2}} (\beta + \sigma k) / N \mathbf{k} \} \end{aligned} \quad 7.1$$

Using the observed values of σ and k and the corresponding value for $(gh)^{\frac{1}{2}}$, the local group velocity vector at the band center is estimated to be:

$$\mathbf{C}_g = 16 \text{ cm/sec } \mathbf{i} - 0.014 \text{ cm/sec } \mathbf{k} .$$

Sketches of the local group velocity and wavenumber vectors are shown in Figure 11. The group velocity is directed eastward and downward while the wavenumber is directed westward and upward.

The local energy flux vector \mathbf{F} may now be estimated from:

$$\mathbf{F} = \bar{E} \mathbf{C}_g , \quad 7.2$$

where \bar{E} is the integrated energy density across the frequency band of interest. The energy density is entirely kinetic on the equator since the oscillations are symmetric. Therefore \bar{E} is computed from the v component variance resulting in:

$$\mathbf{F} = 260 \text{ ergs/cm}^2 \text{ sec } \mathbf{i} - 0.23 \text{ ergs/cm}^2 \text{ sec } \mathbf{k} .$$

The energy flux vector becomes meaningful when we consider the dimensions of the wave packet. By integrating the flux vector over the packet, an estimate of the energy transport in the zonal and vertical directions per unit crest width (meridional direction) may be obtained. Estimates of packet dimensions are largely heuristic due to the limited array size; however, the results are reasonable and self consistent. For

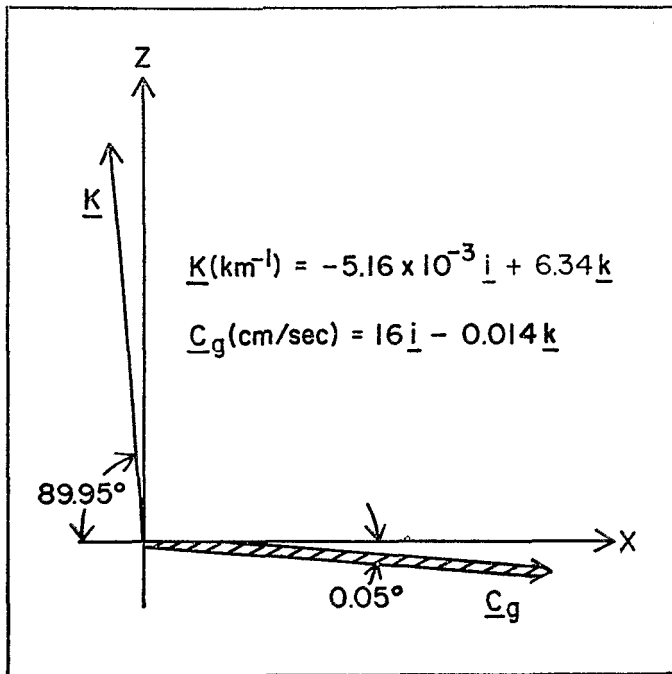


Figure 11. Sketches of the wavenumber and group velocity vectors estimated at the band central frequency.

a wavenumber bandwidth limited process, the spatial modulation in x has the form of $\sin(\Delta kx/2)/(\Delta kx/2)$ and the e -folding scale in amplitude is approximately $2e/\Delta k$ (similarly for z with the wavenumber bandwidth Δk replaced by Δm). The wavenumber component bandwidths Δk and Δm obtained from the Fourier coefficients across the frequency band of interest are $2.17 \times 10^{-3} \text{ km}^{-1}$ and 4.38 km^{-1} respectively; which transform to e -folding amplitude scales of $\Delta x = 2500 \text{ km}$ and $\Delta z = 1200 \text{ m}$ respectively. Using these values, the energy transport in the zonal and vertical directions ($F_z \Delta Z$ and $F_x \Delta x$) per unit crest width are roughly the same and sum to $9 \times 10^7 \text{ ergs/cm sec}$. For comparison, the energy transport in a surface gravity wave field of 0.5 m amplitude and 9 sec period is about $8 \times 10^8 \text{ ergs/cm sec}$. Therefore, the energy transport for the observed equatorially trapped Rossby-gravity waves appears to be within an order of magnitude of that for a modest surface gravity wave field characteristic of the equatorial area.

b. Material rate of change. A self consistency may be shown between the observed local rate of change of energy and that computed using the group velocity and packet dimensions above. Neglecting sources, dissipation and nonlinear interactions, the radiative transfer equation reduces to:

$$\frac{\partial E}{\partial t} + \mathbf{C}_g \cdot \nabla E = 0, \quad 7.3$$

i.e. the material rate of change of energy following the wave packet is zero. The spatial gradient in energy density may be estimated by the wavenumber bandwidth energy e -folding scales: $\delta x = 2e^{1/2}/\Delta k$ and $\delta z = 2e^{1/2}/\Delta m$, and a local e -folding time scale Δt then follows from:

$$-\Delta t = \left(\frac{C_{gz}}{\delta x} + \frac{C_{gz}}{\delta z} \right). \quad 7.4$$

Using values in section 7a, we calculate Δt to be about 40 days, or slightly more than one period. This e -folding scale estimated under the assumption of linear wave propagation past a fixed point agrees very well with the observation of approximately three complete cycles shown in Figure 4. The corresponding (and independently arrived at) e -folding time scale using the frequency bandwidth is 45 days.

8. Discussion

a. Related observations. We have focused upon a six month subset owing to the availability of data for analysis in three dimensions. However, oscillations of the type described were present (with some frequency and amplitude modulation) during the full 18 month sample at 0N, 3W. Very similar oscillations were also reported by Weisberg *et al.* (1979) at 28W during GATE. The wave kinematics were qualitatively the same as shown here; they exhibited westward and upward phase propagation; and their crudely estimated (from 2 month long records) period, zonal wavelength, and wavenumber slope were 36 days, 1500 km, and 10^8 respectively. Harvey and Patzert (1976) reported near bottom westward propagating disturbances in the eastern equatorial Pacific with an approximate 25 day periodicity. Legeckis (1977), using satellite imagery, showed intermittent signatures with a periodicity and wavelength of roughly one month and 1000 km propagating westward along the thermal front separating the Pacific Equatorial Counter Current and South Equatorial Current, and Wyrтки (1978) related these to drifter buoy and sea level observations. It appears that forced waves of this nature are a fairly ubiquitous feature of the tropics and Philander (1978b) has suggested that they result from instabilities of the large scale zonal equatorial ocean circulation.

b. Energy considerations. The consistency shown between the local rate of change of wave energy following a packet and the observations suggest that nonlinear interactions are relatively unimportant (at the observational depth below regions of high shear). Excepting dispersion, it follows that the waves should be capable of propagating without change in form. Given the group velocity vector and its variation with the buoyancy frequency, the wave energy can travel several thousand kilometers zonally before encountering the bottom. Therefore, the observed Rossby-gravity

waves may be capable of communicating energy over large zonal distances possibly affecting eastern boundary processes.

The net energy transport of a wave packet depends upon its dimensions. Therefore, time dependence (e.g. seasonal) and modulation are important factors. Calculating net energy transport involves averages of the flux vector. Since $\langle F \rangle = \langle \bar{E} C_g \rangle$ and not $\langle \bar{E} \rangle \langle C_g \rangle$; where $\langle \rangle$ denotes a time average, care must be exercised in computing net energy flux. The quantity $\langle \bar{E} \rangle \langle C_g \rangle$ results from averages performed over a full record length; whereas the appropriate quantity $\langle \bar{E} C_g \rangle$ may be calculated piecewise by averaging over the modulation time scale and then averaging the pieces. Herein we have presented one such piece.

c. Role of the zonal African coast. The role of the zonal African coast upon equatorially trapped waves and the effects of the waves upon coastal processes have been topics of recent interest. Since the trapping scale for the observed oscillations was only 210 km they were unaffected by the coast and the modifications to the wave field suggested by Philander (1977) did not apply in this particular case. Whether or not this occurs over other portions of the spectrum will be addressed in the continued analysis of the data set.

9. Summary and conclusions

A collaborative field experiment involving U.S. and French oceanographers has been on-going in the Gulf of Guinea since June 1976. Moored current meter records have been collected for the study of equatorially trapped waves, their effects upon the medium through which they propagate, and the effect of the zonal African coast upon them. The most conspicuous features observed in 18 months of data viewed thus far are fairly regular (through frequency and amplitude modulated) oscillations with a time scale of about one month. The present paper has focused solely upon the frequency band encompassing this dominant process. A six month subset of the data having three dimensional coverage has been analysed. Future papers will treat other portions of the spectrum.

The oscillations have been ascribed to packets of zonally and vertically propagating equatorially trapped Rossby-gravity waves. They were coherent over the array: 126 km zonally, 57 km meridionally, and 300 m vertically; with band central values for period, zonal wavelength, and vertical wavelength of 31 days, 1220 km, and 990 m respectively. The observed phase propagation was westward and upward while the calculated group velocity was eastward and downward.

Kinematical consistencies were developed between the observations and a symmetric equatorially trapped wave mode. The velocity components were shown to be coherent and rectilinearly polarized on the equator while being coherent and clockwise elliptically polarized north of the equator. The ellipses were stable with semi-major axis oriented north-south.

Wavenumber vector analysis was performed in three dimensions followed by a refinement in two dimensions after the meridional wavenumber component was shown to be zero. A kinematical test of the wavenumber irrotationality was then shown to be valid over the frequency band of interest.

Given the kinematical descriptions we then analyzed three independent dynamical consistencies between the observations and the Rossby-gravity wave model: (1) the vertical wavenumber component determined from the observed zonal wavenumber component via the vertical structure equation, (2) the zonal wavenumber component determined from the observed vertical wavenumber component via the horizontal structure equation, and (3) the ellipse axis ratio determined from the theoretical eigenfunctions. A fourth check involved the WKB scaling in the vertical. The agreement between the data and theory was excellent in all of the above consistency tests.

Utilizing the dispersion relation for the Rossby-gravity wave we estimated the group velocity vector and the energy transport by the wave packet. The energy transport per unit crest width appeared to be within an order of magnitude of that for a modest surface gravity wave field characteristic of the tropics. The observed local rate of change of wave energy was shown to be consistent with the propagation of the wave packet past a fixed-point suggesting that nonlinear interactions were relatively unimportant at the observational depth.

In conclusion: a packet of zonally and vertically propagating equatorially trapped Rossby-gravity waves has been observed in the Gulf of Guinea. The trapping scale was sufficiently small so that the waves were not affected by the zonal African coast. Waves of this type appear to be a fairly ubiquitous feature of the tropics. Very similar oscillations were observed further to the west in the Atlantic during GATE and evidence for them also exists in the Pacific. The waves seem to be energetic, persistent, and linear and may transport energy over large zonal distances along the equatorial waveguide. Their forcing mechanisms, net energy flux, and effects are important topics for future study.

Acknowledgments. This research was supported by a grant from the National Science Foundation, Oceanography Section, grant number OCE76-09786. Ship time aboard the French vessels N.O. *Capricorne* and N.O. *Nizery* upon which this project depended was provided by the Director General of ORSTOM, Paris. The officers of these vessels and the staff at the Centre de Recherches Oceanographiques, Abidjan, Ivory Coast were most cooperative and helpful. Messrs. T. Pazis, J. Sammons, and M. Mulroney of the electronics group at the Graduate School of Oceanography, University of Rhode Island prepared the instrumentation and assisted with the mooring deployments. Mr. J. Hickman assisted with the computations performed at the North Carolina State University.

REFERENCES

- Fofonoff, N. P. 1969. Spectral characteristics of internal waves in the ocean. *Deep-Sea Res.*, 16, 59-71.
- Gonella, J. 1972. A rotary-component method for analyzing meteorological and oceanographic vector time series. *Deep-Sea Res.*, 19, 833-846.

- Harvey, R. R. and W. C. Patzert. 1976. Deep current measurements suggest long waves in the eastern equatorial Pacific. *Science*, 193, 883-884.
- Holton, J. R. 1975. *The Dynamical Meteorology of the Stratosphere and Mesosphere*, Meteorological Monographs. American Meteorological Society, Boston, Mass., 15, 37.
- Legeckis, R. 1977. Long waves in the eastern equatorial Pacific Ocean: A view from a geostationary satellite. *Science*, 197, 1179-1181.
- Lighthill, M. J. 1969. Dynamic response of the Indian Ocean to the onset of the southwest monsoon. *Phil. Trans. Roy. Soc. London (A)*, 265, 45-92.
- Lindzen, R. S. and T. Matsuno. 1968. On the nature of large scale wave disturbances in the equatorial lower stratosphere. *J. Met. Soc. Japan*, 46, 3, 215-220.
- Matsuno, T. 1966. Quasi-geostrophic motions in the equatorial area. *J. Met. Soc. Japan*, 44, 25-43.
- Moore, D. W. and S. G. H. Philander. 1977. Modelling of the tropical oceanic circulation, in *The Sea*, vol. 7, E. D. Goldberg *et al.* ed., Wiley-Interscience, New York, 1048.
- Mooers, C. N. K. 1973. A technique for the cross spectrum analysis of pairs of complex-valued time series, with emphasis on properties of polarized components and rotational invariants. *Deep Sea Research*, 20, 1129-1141.
- Philander, S. G. H. 1977. The effects of coastal geometry on equatorial waves (forced waves in the Gulf of Guinea), *J. Mar. Res.*, 35, 509-523.
- 1978a. Forced oceanic waves. *Rev. Geophys. & Space Phys.*, 16, 15-46.
- 1978b. Instabilities of equatorial currents, Part II. *Jour. Geophys. Res.*, 83, C7, 3679-3682.
- Phillips, O. M. 1977. *The Dynamics of the Upper Ocean*, 2nd edition, Cambridge University Press, Cambridge, 336 pp.
- Thompson, R. O. R. Y. 1977. Observations of Rossby waves near site D. *Prog. Oceanogr.*, 7, 135-162.
- Weisberg, R. H., L. Miller, A. Horigan and J. A. Knauss. 1979. Velocity observations in the equatorial thermocline during GATE. *Deep Sea Research*, in press.
- Wyrtki, K. 1978. Lateral oscillations of the Pacific Equatorial Counter-current. *J. Phys. Oceanogr.*, 8, 530-532.
- Yanai, M. and T. Maruyama. 1966. Stratospheric wave disturbances propagating over the equatorial Pacific. *J. Met. Soc. Japan*, 44, 291-294.

Received: 12 July, 1978; revised: 13 October, 1978.

3

4

5

6

Printed in U.S.A. for the Sears Foundation for Marine Research,
Yale University, New Haven, Connecticut, 06520, U.S.A.
Van Dyck Printing Company, North Haven, Connecticut, 06473, U.S.A.